

Cite this: DOI: 10.1039/xxxxxxxxxx

Testing the Wyart-Cates model for non-Brownian shear thickening using bidisperse suspensions

Ben M. Guy,^a Christopher Ness,^{b,c} Michiel Hermes,^{a,d} Laura J. Sawiak,^a Jin Sun,^b and Wilson C. K. Poon^a

Received Date
Accepted Date

DOI: 10.1039/xxxxxxxxxx

www.rsc.org/journalname

There is a growing consensus that shear thickening of concentrated dispersions is driven by the formation of stress-induced frictional contacts. The Wyart-Cates (WC) model of this phenomenon, in which the microphysics of the contacts enters solely via the fraction f of contacts that are frictional, can successfully fit flow curves for suspensions of weakly polydisperse spheres. However, its validity for “real-life”, polydisperse suspensions has yet to be seriously tested. By performing systematic simulations and experiments on bidisperse mixtures of spheres, we show that the WC model applies only in the monodisperse limit and fails when substantial bidispersity is introduced. Our results prompt new questions about the microphysics of thickening for both monodisperse and polydisperse systems.

1 Introduction

Shear thickening, the increase in viscosity η with shear stress σ or rate $\dot{\gamma}$, is ubiquitous in concentrated suspensions¹. Its microscopic origin has been hotly debated². Recent experiments^{3–7}, simulations^{8,9} and theoretical modelling¹⁰ point to a σ -dependent transition from frictionless (sliding) to frictional (rolling) inter-particle contacts. A phenomenological model by Wyart and Cates¹⁰ (WC) predicts thickening based on a single microphysical parameter, the fraction of frictional contacts, f . It fits well the rheology of model systems^{3,5}; however, its validity for complex industrial suspensions remains untested. We systematically explore the conditions under which the WC model breaks down for one kind of complexity: size polydispersity, and reveal important shortcomings in our current understanding of shear thickening.

The phenomenology is generic^{3,5,11}. Figure 1(a) shows literature flow curves, $\eta(\sigma)$, for buoyancy-matched suspensions of polymethylmethacrylate (PMMA) spheres with diameter $d \approx 4\mu\text{m}$ at different volume fractions ϕ^3 . At any fixed σ (vertical lines), the viscosity increases with ϕ , Fig. 1(b) (symbols). The viscosity

“branches” at different σ are well described by

$$\eta/\eta_f = (1 - \phi/\phi_J)^{-2}, \quad (1)$$

which diverges at a σ -dependent jamming volume fraction $\phi_J(\sigma)$; η_f is the solvent viscosity. Figure 1(b) shows example fits of Eq. 1 (lines) with ϕ_J as a free parameter. The fitted $\phi_J(\sigma)$, Fig. 1(c), is a decreasing function of σ ; so, increasing σ at fixed ϕ , i.e., traversing a vertical path in Fig. 1(b) (arrow), decreases ϕ_J and causes η to increase: the suspension shear thickens, Fig. 1(a). The limiting low- and high- σ viscosity plateaux, η_0 and η_m [blue and red in Fig. 1(b)], diverge at ϕ_0 and $\phi_m < \phi_0$, respectively.

There is evidence of this scenario in a range of experimental systems^{3,5,11}. The precise values of ϕ_0 and ϕ_m , and the form of $\phi_J(\sigma)$ [and hence $\eta(\sigma)$], depend on details of particle shape¹², size polydispersity¹¹ and surface roughness^{13,14}. In all systems, shear-induced jamming¹⁵, inhomogeneous flow (shear banding)¹⁶ or unsteady flow¹⁷ are observed for $\phi_m \leq \phi < \phi_0$, where conditions exist for which $\phi > \phi_J$, Fig. 1(c), i.e., the system can exhibit solid-like behaviour.

In the WC model¹⁰, inter-particle contacts are either lubricated, with static friction coefficient $\mu = 0$, or frictional, with $\mu > 0$. The fraction of the latter, f , increases with σ , Fig. 2(a). WC’s jamming volume fraction is a function of f only:

$$\phi_J^{\text{WC}} = f\phi_m + (1 - f)\phi_0, \quad (2)$$

changing linearly from random close packing, ϕ_0 , at $f = 0$ (all lubricated contacts) to frictional jamming, ϕ_m , at $f = 1$ (all frictional contacts), Fig. 2(b). Thus, $\phi_J^{\text{WC}}(f(\sigma))$ decreases with σ , Fig. 2(c), and determines η via some empirical form, e.g., Eq. 1^{3,5}, leading

^a School of Physics and Astronomy, University of Edinburgh, King’s Buildings, Peter Guthrie Tait Road, Edinburgh EH9 3FD.

^b School of Engineering, University of Edinburgh, King’s Buildings, Peter Guthrie Tait Road, Edinburgh EH9 3JL

^c Department of Chemical Engineering and Biotechnology, University of Cambridge, Cambridge CB3 0AS, UK.

^d Soft Condensed Matter, Debye Institute for Nanomaterials Science, Utrecht University, Princetonplein 5, 3584 CC Utrecht, The Netherlands

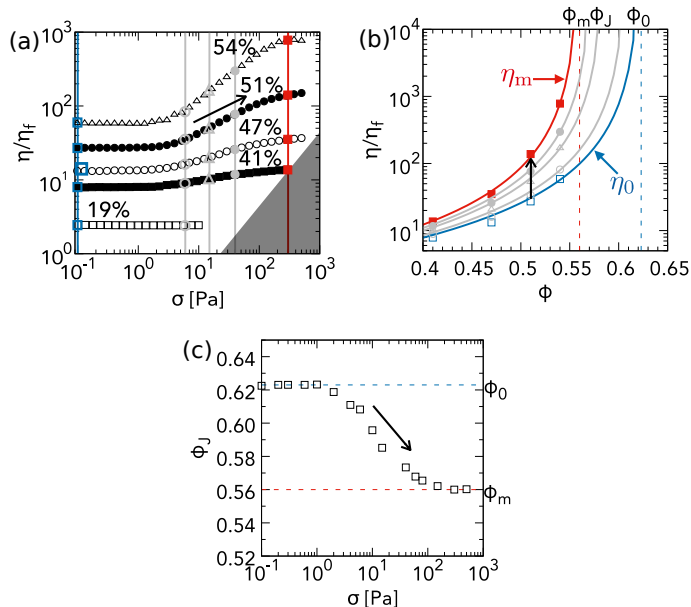


Fig. 1 Experimental shear thickening phenomenology. (a) Relative viscosity η/η_f as a function of shear stress σ at different volume fractions ϕ (as labelled) for $d = 3.78\mu\text{m}$, PHSA-stabilised, PMMA spheres in a cyclohexylbromide-decalin mixture of viscosity $\eta_f = 2.83 \times 10^{-3}\text{Pa s}$ (taken from Guy *et al.*³). The grey region is inaccessible due to inertial edge fracture. (b) Symbols, viscosity “branches” for different (fixed) values of σ in (a). Lines correspond to fits by eye to Eq. 1. The jamming volume fraction at which each viscosity branch diverges, ϕ_j , depends on σ . Blue and red lines and symbols correspond respectively to the limiting low- σ and high- σ viscosities, η_0 and η_m . (c) $\phi_f(\sigma)$, obtained from the fits shown in (b). $\phi_f(\sigma)$ decreases smoothly from ϕ_0 , the ϕ at which η_0 diverges, to ϕ_m , the ϕ at which η_m diverges. In all parts: shear thickening arises at any ϕ , e.g., $\phi = 0.51$, because increasing σ decreases ϕ_f [black arrow in (c)], shifting the viscosity branch in (b) to the left and so increasing η [black arrows in (b) and (a)].

to shear-thickening flow curves, Fig. 2(d) (line).

The WC model, Eq. 1-2, predicts the σ - and ϕ - dependent viscosity, $\eta^{\text{WC}}(\sigma, \phi)$, from three inputs: the limiting frictionless and frictional jamming points, ϕ_0 and ϕ_m , and the σ -dependent fraction of frictional contacts, f . ϕ_m and ϕ_0 , can be obtained by fitting viscosity branches at different σ , as done in Fig. 1(b). They are not related to shear thickening *per se*. On the other hand, f , which determines the shape of the flow curve, is currently inaccessible in experiments. Thus, various *ansatzs* are used to fit the WC model to experiments. For sterically-stabilised PMMA spheres, Guy *et al.*³ used a ϕ -independent sigmoidal form:

$$f(\sigma) = \exp[-(\sigma^*/\sigma)^\beta], \quad (3)$$

with $\beta = 0.85$. The single stress scale here, σ^* , is proportional to the “engineering” onset stress at which $\eta(\sigma)$ visibly begins to increase. Guy *et al.* found $\sigma^* \propto d^{-2}$, suggesting $\sigma^* \propto F^*/d^2$ where $F^* \sim k_B T/\text{nm}$ is a constant force¹⁰. Royer *et al.*⁵ used a similar form to fit data for dispersions of charge-stabilised silica.

In discrete-element (DEM) simulations, f can be calculated directly from particle coordinates. A popular choice is to use the “critical-load model” (CLM), in which μ jumps from 0 to > 0 when the normal contact force between particles, F , exceeds a thresh-

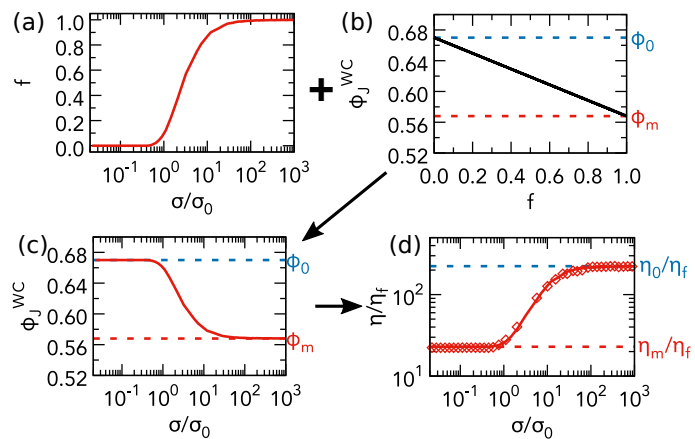


Fig. 2 Logic of the WC shear thickening model. (a) The fraction of frictional contacts, f , takes a sigmoidal form. (b) $\phi_j^{\text{WC}}(f)$ is linearly interpolated between ϕ_0 at $f = 0$ to ϕ_m at $f = 1$. (c) The previous two plots directly give $\phi_j^{\text{WC}}(f(\sigma))$, which is inverse sigmoidal. (d) Using $\phi_j^{\text{WC}}(f(\sigma))$ in Eq. 1 gives $\eta(\sigma)$, which shows shear thickening (line). *Testing the WC model using simulations.* The plot in (a) is calculated directly using contact forces from simulations of pure small-sphere suspension at $\phi = 0.53$. See the text for how we obtain values for ϕ_0 and ϕ_m to calculate the $\phi_j^{\text{WC}}(f)$ plotted in (b) from Eq. 2. These two plots directly give the ϕ_j^{WC} in (c), which, when used in Eq. 1 gives the flow curve in (d), $\eta^{\text{WC}}(\sigma)$ (line). The symbols in (d) are the computed viscosity from simulations.

old value, F^* (the critical load). This model reproduces⁹ the phenomenology of Fig. 1 and unstable flow at high ϕ . For a bidisperse mixture of spheres with diameter d_1 and $d_2 = d_1/1.4$, Mari *et al.* found⁹ a ϕ -independent $f(\sigma)$ of the form Eq. 3, with $\beta = 1.1$ and $\sigma^* \approx F^*/[6\pi(d_2/2)^2]$, and later used it to fit flow curves at a range of ϕ ¹⁸. Thus, in this one case, the WC model is fully validated: the measured fraction of frictional contacts used in Eq. 2 correctly predicts the viscosity. The similarity between the forms of $f(\sigma)$ used to fit experiments and measured in simulations suggests that f in mildly-polydisperse experimental systems can indeed be well described by Eq. 3 or some similar form.

In these studies, a weak polydispersity (= standard deviation normalised by the mean of the particle size distribution) $s \lesssim 20\%$ is used to inhibit shear-induced crystallisation⁹. Industrial dispersions typically have broad, often multimodal, size distributions with $s \gtrsim 100\%$. The low- s phenomenology in Fig. 1 appears also to hold for such industrial systems^{11,19–21}, but the validity of WC theory in these more complex suspensions has not been tested.

Indeed, it is a surprise for the WC model to work, and work well, even for low- s systems. In suspension rheology, details of the microstructure, fabric of the contact network and distribution of forces matter. Cates pointed out long ago that the relatively small number of nearest neighbours, $\sim \mathcal{O}(10)$, usually precludes any mean-field description²². The success of his shear-thickening model with Wyart contradicts this norm: in the WC model, $\eta(\sigma)$ is controlled primarily by a single scalar parameter f that is agnostic to exact microstructural details. For this reason alone, it is important to test the limitations of the WC model, which are, of course, also important for industrial applications.

We systematically test the validity of the WC model in suspensions of strongly bidisperse spheres. As before^{9,18}, we use DEM

simulations to extract $f(\sigma)$ for different mixtures and compare the predictions of the WC model to bulk flow curves. We then use the same $f(\sigma)$ to test the model against experimental data for bidisperse PMMA spheres. We find that WC works for nearly-monodisperse suspensions [i.e., the simulated $f(\sigma)$ correctly predicts $\eta(\sigma)$] but fails in general for bidisperse suspensions. Our results highlight a number of unresolved issues in the current understanding of shear thickening and in the use of the WC framework to make inferences about microphysics. We propose directions for future research to address these issues.

2 Methods

A binary mixture of spheres is characterised by four parameters: $d_1, d_2 < d_1$, the fraction of small particles $\xi = V_2/(V_1 + V_2)$ (where V_1 and V_2 are the total volumes of large and small particles, respectively) and the total volume fraction $\phi = (V_1 + V_2)/V$ (where V is the total volume). We fix ϕ and the size ratio $\alpha \equiv d_2/d_1 \approx 0.25$, and vary ξ . At our α , the small spheres are slightly too large to fit inside four touching large spheres (for which $\alpha_{\max} = 0.225$).

We sheared $N = 2000$ bidisperse, repulsive spheres at fixed ϕ in a periodic cell with Lees-Edwards boundary conditions. Short-range lubrication and repulsive contact forces described by linear springs of stiffness k were resolved using a classical DEM code that allows marginal overlaps δ between the surfaces of pairs of particles²³. We employed a contact model⁹ in which Coulomb friction with static friction coefficient $\mu = 1$ appears beyond a critical overlap δ^* , corresponding to a critical normal load $F^* = k\delta^*$. For simplicity, and consistency with experiments for nearly-monodisperse systems³, we use a constant F^* (and hence δ^*) that is independent of d_1 and d_2 .

Our unit of stress is $\sigma_0 = F^*/(3\pi d_2^2/2)$, at which purely small particles ($\xi = 1$) shear thicken⁹; pure large spheres shear thicken at $\sim \alpha^2 \sigma_0$. For bidisperse mixtures, we averaged σ over the strain interval $\gamma \in [1.5, 3]$ or $\in [1.5, 2]$, in which the system had reached steady state for all ξ . For monodisperse suspensions, we averaged over $\gamma \in [0.7, 1]$ to avoid the onset of large-scale crystallization²⁴.

We performed experiments on binary suspensions of PMMA spheres stabilised with poly-12-hydroxystearic acid (PHSA) in a near-density-matching mixture of cyclohexylbromide and decalin (density $\approx 1.18 \text{ g cm}^{-3}$, viscosity $\eta_f = 2.4 \text{ mPa s}$). We varied ξ at a fixed $\phi = 0.51$ by mixing together monomodal suspensions with mean particle diameters $d_2 = 0.712 \mu\text{m}$ and $d_1 = 2.76 \mu\text{m}$ and $s \approx 10\%$ (from static light scattering). Flow curves were measured using an Anton Paar MCR 301 rheometer with sandblasted steel cone (angle 1° , diameter 50 mm , roughness $\sim 10 \mu\text{m}$) and roughened aluminium base plate (roughness $\sim 10 \mu\text{m}$) at 20°C . A solvent trap minimised evaporation.

3 Results

3.1 Bidisperse shear thickening phenomenology

We first present the simulated relative viscosity η/η_f as a function of shear stress σ/σ_0 for fixed $\phi = 0.53$ and $\alpha = 0.25$ at various fractions of small particles, Fig. 3(a), $\xi = 0$ (pentagon), 0.2 (\square), 0.5 (∇), 0.65 (\triangle), 0.8 (\circ) and 1 (\diamond). Bidisperse and monodisperse flow curves are qualitatively similar, showing shear thick-

ening between two Newtonian plateaux. Figure 3(b) shows the ξ -dependent plateau viscosities, $\eta_0(\xi)$ (\blacksquare) and $\eta_m(\xi)$ (\blacksquare), estimated by eye from Fig. 3(a). Mixing particles reduces both limiting viscosities relative to the values for single-sized spheres. Such a ‘‘Farris effect’’²⁵ has been widely observed in fixed-friction (i.e., Newtonian) suspensions^{25,26}. The limiting volume fractions, $\phi_0(\xi)$ and $\phi_m(\xi)$, Fig. 3(c) (\blacksquare and \blacksquare respectively), are calculated using the simulated η_0 and η_m values in Eq. 1 with $\phi = 0.53$. The non-monotonic behaviour directly mirrors that of $\eta_0(\xi)$ and $\eta_m(\xi)$.

Experimental flow curves for binary mixtures of PMMA with $\alpha = 0.26$ and $\phi = 0.51$, Fig. 3(d), show similar phenomenology, except that the limiting high- σ behaviour is preempted by edge fracture due either to an inertial instability (grey region), or a different fracture mechanism when σ exceeds $\approx 10^3 \text{ Pa}$. Thus, we cannot access $\eta_m(\xi)$ directly for all ξ . Shear thickening is preceded by shear thinning, presumably due to residual Brownian motion³; so, we estimate η_0 by the viscosity minimum before the onset of thickening, Fig. 3(b) (\circ). The experimental $\eta_0(\xi)$ show the same non-monotonicity as the simulated values, but are always too high, by up to a factor of $\lesssim 2$ for the two end members ($\xi = 0$ or 1). Using the experimental values of $\eta_0(\xi)$ in Eq. 1 with $\phi = 0.53$ gives us an experimental estimate of $\phi_0(\xi)$, Fig. 3(c) (\circ). Consistent with the experimental viscosities $\eta_0(\xi)$ being higher than simulated values, the experimentally deduced $\phi_0(\xi)$ are somewhat lower than the simulated values, i.e. the experimental system at $\phi = 0.53$ is closer to jamming than the corresponding simulated system.

3.2 Comparing simulations to the WC model

We test the WC model by comparing simulated flow curves, $\eta(\sigma)$, with those calculated using the fraction of frictional contacts, $f(\sigma)$, measured from the simulations, $\eta^{\text{WC}}(\sigma)$. To explain our procedure, consider data for monodisperse small particles ($\xi = 1$). First, we calculate $f(\sigma)$ directly from inter-particle forces by counting, at each σ , the fraction of contacts with $F > F^*$. The $f(\sigma)$ so obtained, Fig. 2(a), is sigmoidal, similar to the $f(\sigma)$ in bidisperse mixtures with $\alpha = 0.71$ ⁹ and Eq. 3.

To calculate $\phi_j^{\text{WC}}(f)$ from Eq. 2, we need ϕ_0 and ϕ_m , which could be obtained by simulating and fitting $\eta(\sigma, \phi)$ at a range of ϕ , as done in Fig. 1. Instead, we use our simulated values of the low- and high- σ viscosities, η_0 and η_m , at $\phi = 0.53$ in Eq. 1 to obtain ϕ_0 and ϕ_m , giving the $\phi_j^{\text{WC}}(f)$ in Fig. 2(b).

From $f(\sigma)$, Fig. 2(a), and $\phi_j^{\text{WC}}(f)$, Fig. 2(b), we now calculate $\phi_j^{\text{WC}}(f(\sigma))$, Fig. 2(c), which decreases smoothly from $\approx \phi_0$ at $\sigma/\sigma_0 \ll 1$ to ϕ_m at $\sigma/\sigma_0 \gg 1$. Finally, we calculate the viscosity by substituting $\phi_j^{\text{WC}}(f(\sigma))$, Fig. 2(c), into Eq. 1. The flow curve, $\eta^{\text{WC}}(\sigma)$, Fig. 2(d) (solid line), increases smoothly from η_0 to η_m .

We compare this flow curve calculated using the measured $f(\sigma)$ with the simulated $\eta(\sigma)$, Fig. 2(d) (symbols). The two calculated plateaux agree with the simulated values by construction. The WC model is judged instead by how well it captures the shear thickening process. It does this well for monodisperse spheres. Both model-predicted and simulation viscosities start to increase at $\sigma/\sigma_0 \approx 1$, reaching saturation at $\sigma/\sigma_0 \gtrsim 30$.

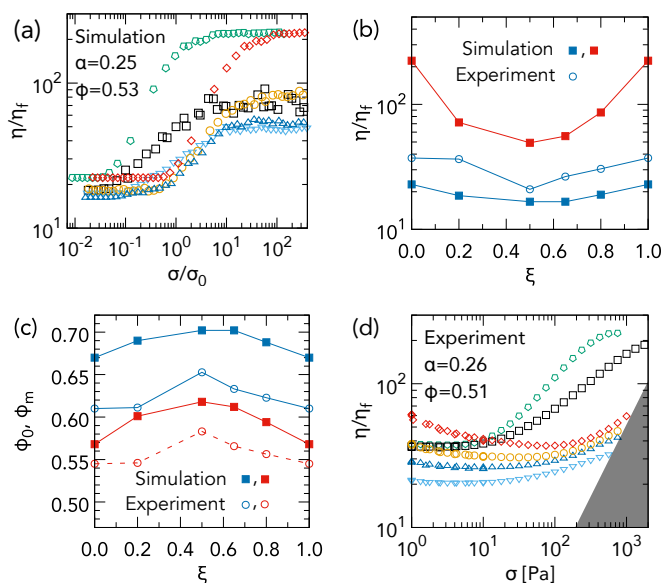


Fig. 3 Bidisperse shear thickening phenomenology. (a) η/η_f as a function of σ/σ_0 from simulations at $\alpha = 0.25$ and $\phi = 0.53$, with $\xi = 0$ (pentagon), 0.2 (\square), 0.5 (∇), 0.65 (\triangle), 0.8 (\circ) and 1 (\diamond). (b) Frictionless relative viscosity η_0/η_f from simulations (—■—) and experiments (—○—), and frictional relative viscosity η_m/η_f from simulations (—■—). (c) Limiting jamming volume fractions, ϕ_0 (blue) and $\phi_m < \phi_0$ (red), versus ξ from simulations (—■—, —■—) and experiments (—○—, —○—). (d) Experimental η/η_f versus σ for PMMA spheres at $\alpha = 0.26$ and $\phi = 0.51$, with $\xi = 0$ (pentagon), 0.2 (\square), 0.5 (∇), 0.65 (\triangle), 0.8 (\circ) and 1 (\diamond). Inertial fracture at $\dot{\gamma} \approx 8 \times 10^3 \text{ s}^{-1}$ renders the grey-shaded region inaccessible³.

We repeat this procedure for our bidisperse suspensions with $\xi = 0.2, 0.5, 0.65$ and 0.8 . Again, the measured $f(\sigma)$, Fig. 4(a), and linearly interpolated $\phi_j^{\text{WC}}(f)$, Fig. 4(b), are used to calculate $\phi_j^{\text{WC}}(\sigma)$, Fig. 4(c), from which we obtain flow curves, Fig. 4(d) (lines). We compare these with the simulated viscosities, Fig. 4(d) (symbols), recalling that the limiting viscosities are constrained to fit, and noting that data for different ξ have been shifted vertically to aid visibility (see caption for shift factors).

Note, first, that $f(\sigma)$ for the monodisperse end members, $\xi = 0$ and 1 , are identical in shape, Fig. 4(a), but with the former shifted to the left by a factor of $(d_2/d_1)^2 = \alpha^2 = 0.0625$ due to a decrease in σ^* by the same factor for the larger particles³. Addition of just 20% of small spheres to a suspension of large spheres ($\xi = 0.2$) produces a dramatic effect, Fig. 4(a). While frictional contacts still start to form at $\sigma_1^* \approx 0.06\sigma_0$, the onset is now much more gradual, until $\sigma \approx \sigma_2^* \approx \sigma_0$, whereupon $df/d\sigma$ abruptly becomes as large as the monodisperse case (either $\xi = 0$ or 1), before f saturates at a σ that is comparable to (but slightly later than) that of monodisperse small spheres, even though only 20% of these are present. By $\xi = 0.5$, $f(\sigma)$ becomes very similar to that of that of monodisperse small spheres ($\xi = 1$); although, the onset is still clearly somewhat earlier and the saturation somewhat lower. These features become progressively less obvious at $\xi = 0.65$ and 0.80 . The effect of bidispersity is therefore asymmetrical: the presence of 20% of large spheres in 80% of small spheres has far smaller an effect on $f(\sigma)$ than the reverse situation.

Turning to the shear-thickening flow curves, Fig. 4(d), we see

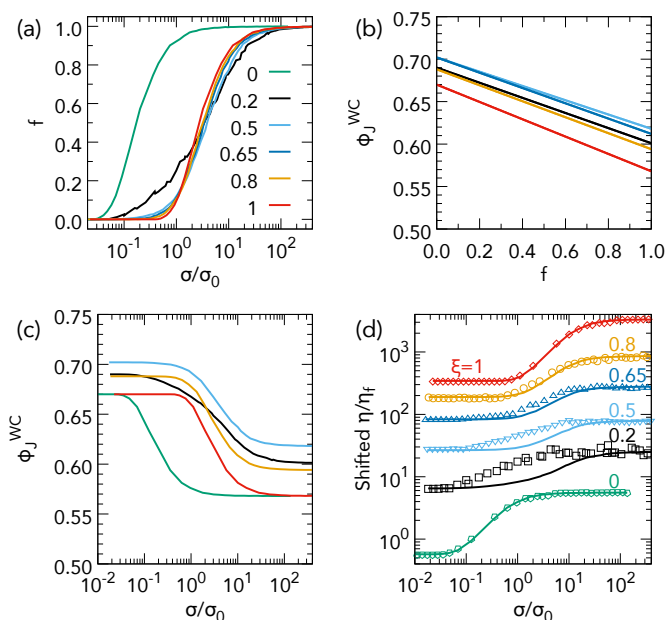


Fig. 4 Failure of the WC model for bidisperse simulations. (a) Fraction of frictional contacts f as a function of σ/σ_0 , extracted from simulations at different ξ , as labelled. (b) WC jamming volume fraction, ϕ_j^{WC} , as a function of f for different ξ [colours as in part (a)]. (c) ϕ_j^{WC} as a function of σ calculated using (b) and $f(\sigma)$ from (a). (d) Symbols: shifted flow curves for different ξ , as labelled. Shift factors are: $\xi = 0$, 0.025; $\xi = 0.2$, 0.35; $\xi = 0.5$, 1.6; $\xi = 0.65$, 5; $\xi = 0.8$, 10 and $\xi = 1$, 15. Lines: predictions of the WC model shifted by the same factors.

that, as expected, the WC model reproduces the simulated data for the two monodisperse end members. It gives a tolerable representation of the data at $\xi = 0.8$, i.e. when there are 20% of large spheres present in a predominantly small-sphere system; but, it fails badly in the reverse situation, when there are 20% of small spheres in a mainly large-sphere system ($\xi = 0.2$). The disagreement between the WC prediction and simulation data is still substantial at $\xi = 0.5$, and remains perceptible at $\xi = 0.65$.

3.3 Comparing experiments to the WC model

We do not have experimental access to the fraction of frictional contacts, and the flow curves do not reach the high-viscosity plateau at all ξ . To test the validity of the WC model, we used the $f(\sigma)$ obtained in simulations at each ξ , treating σ_0 (the small-particle onset stress) as a global fitting parameter, and ϕ_m as a local fitting parameter for each ξ . In Fig. 5, we plot measured flow curves (symbols) and WC flow curves (lines) for $\sigma_0 = 250 \text{ Pa}$ and $\phi_m(\xi) = \Lambda\phi_0(\xi)$ with $\Lambda = 0.89$. Choosing a ξ -dependent $\Lambda = \phi_m/\phi_0$ does not affect any of our conclusions. Data and fits have been shifted vertically for clarity (see caption). While the lack of high-stress data for all cases except $\xi = 0$ renders it difficult to be as quantitative as we have been with simulations, all the same trends noted when we compared simulations with the WC model are clearly reproduced here. In particular, there is a striking disagreement between model and experiment at $\xi = 0.2$.

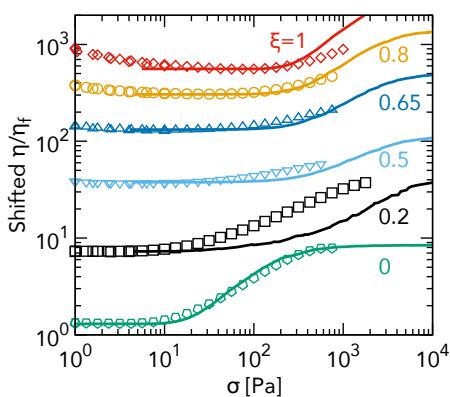


Fig. 5 Failure of the WC model for PMMA spheres. Symbols, shifted flow curves from experiments for different ξ , as labelled. Lines, shifted WC model predictions. Shift factors are: $\xi = 0, 0.035$; $\xi = 0.2, 0.2$; $\xi = 0.5, 1.8$; $\xi = 0.65, 5$; $\xi = 0.8, 10$ and $\xi = 1, 15$.

4 Discussion

Previous experiments and simulations find, and we confirm, that the WC model works well in the quasi-monodisperse limit ($s \lesssim 0.2$)¹⁸. This phenomenological model is designed to reveal the consequences of a simplified set of assumptions in the most perspicuous way, and (according to its authors¹⁰) not meant for the fitting of data. Thus, that it works quantitatively in the small- s limit is itself non-trivial, especially given its mean-field nature²².

It is perhaps unsurprising that we find the WC model fails to account for experiments and simulations for a binary mixture with $\alpha = 0.25$ (size ratio 1:4), which translates, using a previously-proposed definition²⁷, to an effective polydispersity $s_{\text{eff}} = (d_1 - d_2)/(d_1 + d_2) \approx 60\%$. The pertinent question is: precisely where is the WC model failing in this case?

In a monodisperse system, there is a single kind of frictional contact. In a bidisperse system, such contacts are of three kinds: large-large ('11'), large-small ('12'), and small-small ('22'). Figure 6 shows how the fractions of different types of frictional contact, f_{11} , f_{12} and f_{22} (with $f_{11} + f_{12} + f_{22} = f$), develop with stress in our simulated $\xi = 0.2$ system, where we observe maximal discrepancy with the WC model. Not surprisingly, frictional contacts first start to form amongst the large species, at $\sigma_1^* \approx 0.06\sigma_0$; however, this contribution rapidly saturates to $f_{11}^\infty \lesssim 0.1$. The latest frictional contacts to form are the small-small ones: f_{22} does not start to increase until $\sigma_2^* \approx \sigma_0$; but, these saturate to about $f_{22}^\infty \approx 0.4 \gtrsim 4f_{11}^\infty$. Ultimately, the largest contribution is from 'mixed' contacts, $f_{12}^\infty \approx 0.5 \gtrsim 5f_{11}^\infty$, which start to form at $\sigma_{12}^* \approx 0.2\sigma_0$ (perhaps fortuitously close to $\sqrt{\sigma_1^* \sigma_2^*}$).

The WC model applied to our system is blind to the distinctions between these three different types of contact. It assumes that any new frictional contact formed as stress builds up contributes equally to the lowering of ϕ_j^{WC} , and therefore to the viscosity increment via Eqs. 1 and 2. Thus, the fact that $f_{12} \approx f_{22} \gg f_{11}$ means that the WC flow curve for $\xi = 0.2$ is much more similar in

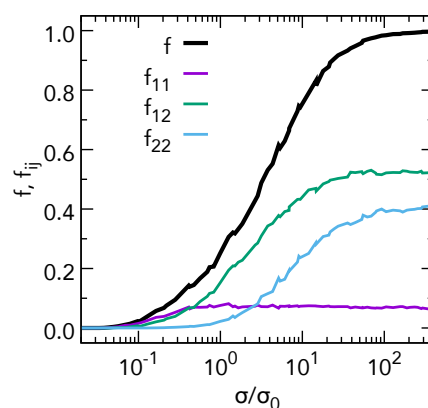


Fig. 6 Simulated σ -dependent fraction of frictional contacts, $f(\sigma)$ (black line), for $\xi = 0.2$ decomposed into contributions from large-large, f_{11} ; large-small, f_{12} and small-small, f_{22} , contacts, as labelled.

shape to the all-small ($\xi = 1$) system than to the $\xi = 0$ system. In reality, both the simulated and experimental flow curves start to shear thicken at σ_1^* , which is where f_{11} starts to increase.

Thus, a basic problem with the WC model applied to our bidisperse system is the equal weighting given to the three kinds of contacts. Instead, many small-large and small-small contacts seem to contribute little to the shift in ϕ_j . This is consistent with a numerical study of static packings of highly polydisperse spheres²⁷, which found spatially heterogeneous force distributions with force transmission dominated by contacts between larger species. It is currently unclear what unequal weighting should be applied, and the physical basis for any such *ansatz*.

Related to, but distinct from, the equal weighting to all kinds of frictional contacts is the indifference to the spatial distribution of these contacts. Simulations by Mari *et al.* show⁹ that this may indeed be true for nearly-monodisperse particles. They found that $f(\sigma)$ was independent of ϕ over the full ϕ -range of thickening ($0.45 \leq \phi \leq 0.56$) for $\alpha = 0.71$, $\xi = 0.5$ bidisperse spheres, even though the contact network is highly anisotropic at low ϕ and isotropic at high ϕ , indicating that thickening is not closely tied to microstructural changes. A systematic study of the angular distribution of '11', '12' and '22' contacts in bidisperse systems would be needed to reveal the specific role of microstructure in polydisperse shear-thickening suspensions.

Finally, the WC model is agnostic to the mechanism whereby frictional contacts increase dissipation (and hence the viscosity). Indeed, a complete physical picture has yet to be established for this link even for fixed- μ (Newtonian) suspensions; although, progress is being made²⁸. One may speculate that some singular feature of monodisperse suspensions renders it possible to ignore this issue in building a model, and that understanding suspensions with industrially realistic degrees of polydispersity may require modelling that includes at least some features of the extra dissipative mechanism brought about by frictional contacts. Thus, e.g., it may be that large-large contacts disproportionately contribute to dissipation, thus explaining their importance in determining the onset of thickening in the $\xi = 0.2$ system seen in both our simulations and experiments.

* A more natural definition would normalise to the average size to give $s \approx 120\%$.

Before concluding, we note that “fitting” the WC model to experimental data with a presumed form for $f(\sigma)$ will result in a $f(\sigma)$ that is *not* the fraction of frictional contacts except in the monodisperse limit^{3,5}.

Summary and conclusions

We have simulated and experimentally measured the rheology of a bidisperse suspension of repulsive spheres to test the validity of the WC model of shear thickening. By using the fraction of frictional contacts f extracted directly from simulations, we showed that the WC model fails in general for bidisperse mixtures but works in the limiting case of a monodisperse suspension.

In practical terms, our results suggest caution when using the WC model as anything other than an empirical fitting tool. Specifically, little, if any, meaning can be ascribed to f extracted from fits to flow curves. On a fundamental level, our work highlights the need for a focussed effort to understand the link between σ -dependent frictional contact formation and dissipation. Existing studies of shear thickening consider either bulk rheology^{3,5} or *ex-situ*, two-particle properties⁶, with little or no concerted effort to bridge the two regimes. We believe that any serious effort to make this link should consider polydispersity from the outset in its own right, rather than merely as a means of mitigating crystallisation. Indeed, our work hints that the monodisperse limit is a singular one, and so cannot be used as a guide to model development for the flow of polydisperse systems.

Conflicts of interest

There are no conflicts to declare.

Acknowledgements

BMG and MH were funded by EPSRC EP/J007404/1. CJN was funded by EPSRC EP/N025318/1 and the Maudslay-Butler Research Fellowship at Pembroke College, Cambridge. LJS was funded by EPSRC SOFI CDT (EP/L015536/1). JS was funded by EPSRC EP/N025318/1 and The Royal Academy of Engineering/The Leverhulme Trust Senior Research Fellowship LT-SRF1617/13/2. WCKP was funded by EPSRC EP/J007404/1 and EP/N025318/1. We thank John Royer and Dan Hodgson for discussions. The simulation makes use of the LF-DEM code published in Mari *et. al.*⁹ and available at https://bitbucket.org/rmari/lf_dem as well as LAMMPS²⁹.

Notes and references

- 1 H. A. Barnes, *J. Rheol.*, 1989, **33**, 329–366.
- 2 E. Brown and H. M. Jaeger, *Rep. Prog. Phys.*, 2014, **77**, 046602.
- 3 B. M. Guy, M. Hermes and W. C. K. Poon, *Phys. Rev. Lett.*, 2015, **115**, 088304.
- 4 N. Y. C. Lin, B. M. Guy, M. Hermes, C. Ness, J. Sun, W. C. K. Poon and I. Cohen, *Phys. Rev. Lett.*, 2015, **115**, 228304.
- 5 J. R. Royer, D. L. Blair and S. D. Hudson, *Phys. Rev. Lett.*, 2016, **116**, 188301.
- 6 J. Comtet, G. Chatté, A. Niguès, L. Bocquet, A. Siria and A. Colin, *Nat. Commun.*, 2017, **8**, 15633.
- 7 C. Clavaud, A. Bérut, B. Metzger and Y. Forterre, *Proc. Natl. Acad. Sci. (USA)*, 2017, **114**, 5147–5152.
- 8 R. Seto, R. Mari, J. F. Morris and M. M. Denn, *Phys. Rev. Lett.*, 2013, **111**, 218301.
- 9 R. Mari, R. Seto, J. F. Morris and M. M. Denn, *J. Rheol.*, 2014, **58**, 1693–1724.
- 10 M. Wyart and M. E. Cates, *Phys. Rev. Lett.*, 2014, **112**, 098302.
- 11 D. J. Hodgson, M. Hermes and W. C. K. Poon, *arXiv preprint*, 2015, **arXiv:1507.08098**, 1–10.
- 12 E. Brown, H. Zhang, N. A. Forman, B. W. Maynor, D. E. Betts, J. M. DeSimone and H. M. Jaeger, *J. Rheol.*, 2010, **54**, 1023–1046.
- 13 L. C. Hsiao, S. Jamali, E. Glynos, P. F. Green, R. G. Larson and M. J. Solomon, *Phys. Rev. Lett.*, 2017, **119**, 158001.
- 14 C.-P. Hsu, S. N. Ramakrishna, M. Zanini, N. D. Spencer and L. Isa, *Proc. Natl. Acad. Sci. (USA)*, 2018, **115**, 5117–5122.
- 15 I. Peters, S. Majumdar and H. Jaeger, *Nature*, 2016, **532**, 214.
- 16 A. Fall, F. Bertrand, D. Hautemayou, C. Mézière, P. Moucheron, A. Lemaître and G. Ovarlez, *Phys. Rev. Lett.*, 2015, **114**, 098301.
- 17 M. Hermes, B. M. Guy, W. C. K. Poon, G. Poy, M. E. Cates and M. Wyart, *J. Rheol.*, 2016, **60**, 905–916.
- 18 A. Singh, R. Mari, M. M. Denn and J. F. Morris, *J. Rheol.*, 2018, **62**, 457–468.
- 19 P. D’Haene and J. Mewis, *Rheol. Acta*, 1994, **33**, 165–174.
- 20 J. Bender and N. J. Wagner, *J. Rheol.*, 1996, **40**, 899–916.
- 21 B. M. Guy, *PhD thesis*, The University of Edinburgh, 2017.
- 22 M. E. Cates, *Annal. Henri Poincaré Suppl. 2*, 2003, **4**, S647–S661.
- 23 C. Ness and J. Sun, *Soft Matter*, 2016, **12**, 914–924.
- 24 A. Sierou and J. Brady, *J. Rheol.*, 2002, **46**, 1031–1056.
- 25 R. Farris, *Transac. Soc. Rheol.*, 1968, **12**, 281–301.
- 26 S. Pednekar, J. Chun and J. F. Morris, *J. Rheol.*, 2018, **62**, 513–526.
- 27 C. Voivret, F. Radjai, J.-Y. Delenne and M. S. El Youssoufi, *Phys. Rev. Lett.*, 2009, **102**, 178001.
- 28 M. Trulsson, E. DeGiuli and M. Wyart, *Phys. Rev. E*, 2017, **95**, 012605.
- 29 S. Plimpton, *J. Comp. Phys.*, 1995, **117**, 1–19.